Testing Masks and Air Filters with Your Smartphones

Bangjie Sun
National University of Singapore
bangjie@comp.nus.edu.sg

Kanav Sabharwal
National University of Singapore
kanav.sabharwal@u.nus.edu

Gyuyeon Kim
Yonsei University
gyuyeon.kim@yonsei.ac.kr

Mun Choon Chan
National University of Singapore
chanmc@comp.nus.edu.sg

Jun Han
Yonsei University
jun.han@yonsei.ac.kr

ABSTRACT

The demand for masks and air filters with effective filtration capabilities is skyrocketing as there are many applications that require protecting users from inhaling air pollutants or hazardous particles. Unfortunately, we are witnessing a surge in the number of counterfeit and substandard filters attributed to malicious and inept manufacturers. Hence, users are left vulnerable in not knowing which products are reliable. Exacerbating the problem, there are diverse filter standards, each with a unique expression for filtration efficiencies, adding to user confusion. Moreover, the average user lacks the necessary tools, techniques, and knowledge to independently verify the filtration efficiency. Specifically, state-of-the-art solutions are lab-based machines that are extremely expensive and difficult to access for the general public. To solve this problem, we propose *FilterOp*, a novel smartphone-based mask and filter testing system. *FilterOp* is a practical solution that allows a user to estimate the *filtration efficiency* of a mask or a filter using only a pair of commodity smartphones. The novelty of *FilterOp* comes from its use of *light absorption* and *scattering* effects, observed when light propagates through the filter. We evaluate *FilterOp* in comprehensive real-world experiments using 256 filter instances across 27 different make-and-model products with varying filtration efficiencies. Comparing our results to those obtained with a state-of-the-art government-certified testing machine, we observe that *FilterOp* yields comparable results with a low mean absolute error of 2.7%, and detects *substandard* products with an overall accuracy of 96%.

CCS CONCEPTS

• **Human-centered computing** → **Smartphones**; **Mobile phones**;
• **Computing methodologies** → **Computer vision**.

KEYWORDS

Mask Testing, Filter Testing, Smartphone Camera

ACM Reference Format:
Bangjie Sun, Kanav Sabharwal, Gyuyeon Kim, Mun Choon Chan, and Jun Han. 2023. Testing Masks and Air Filters with Your Smartphones. In *The 21st ACM Conference on Embedded Networked Sensor Systems (SenSys '23), November 12–17, 2023, Istanbul, Turkiye.* ACM, New York, NY, USA, 15 pages. https://doi.org/10.1145/3625687.3625807

SenSys '23, November 12–17, 2023, Istanbul, Turkiye

ACM ISBN 979-8-4007-0414-7/23/11…$15.00
https://doi.org/10.1145/3625687.3625807

1 INTRODUCTION

There are numerous applications in which users depend on masks and medical devices to safeguard themselves against inhaling air pollutants or hazardous particles, ensuring that they breathe clean air. For example, *face masks* are one of the most prevalent types of protective gear often used in a wide spectrum of settings including healthcare [16, 44], haze and dust protection, professional cleaning [67, 95], and construction [25, 57]. *Gas masks* are another type of protective gear often used when exposed to more hazardous settings including chemical industries [7, 34, 68], firefighting [8, 81], and military operations [37, 79]. Further, *Ventilation Support Systems* are a type of medical device that provides a constant level of air pressure to patients when worn on their faces. For example, *Continuous Positive Airway Pressure (CPAP)* machines are often used by sleep apnea patients to aid with breathing while sleeping at home [15, 58, 59].

While these masks and medical devices serve different purposes, they rely on their *air filters* to effectively filter hazardous particles, chemicals, and/or pathogens, hence delivering clean air to the wearer. Disposable face masks are produced with an embedded filter layer, while reusable face masks, gas masks, and ventilation support systems are designed with replaceable filters. However, for the average user, the task of navigating the market to find suitable and reliable filters is daunting, primarily due to the following factors. ***(1) Counterfeit, Substandard, and/or Mislabeled Products:*** Today's market is plagued with a surge of *counterfeit* and *substandard* products attributed to either malicious or inept manufacturers. For instance, according to the Centers for Disease Control and Prevention (CDC), over 60% of KN95 masks available in the market are deemed substandard, making them unsafe for the intended usage [11, 19, 31, 32, 77, 88]. Furthermore, there are many instances where the masks are *mislabeled* – i.e., they are either labeled improperly or completely lack any labels. [20, 45, 60, 62, 76, 80]. ***(2) Diverse Standards and their Expressions of Filtration Efficiency:*** In addition, there are *diverse standards*, each expressing filtration efficiencies in a distinct manner, leading to considerable confusion among average consumers. For instance, respirators and surgical masks, despite having significantly different filtration efficiencies, often label their packaging with a standardized "95% Particulate Filtration Efficiency (PFE)" [3, 4]. However, it is important to note that the tested particle size for respirators and surgical masks differ (e.g., 0.3 μm and 3.0 μm for respirators and surgical masks, respectively [61]), even though the packaging states the same numerical

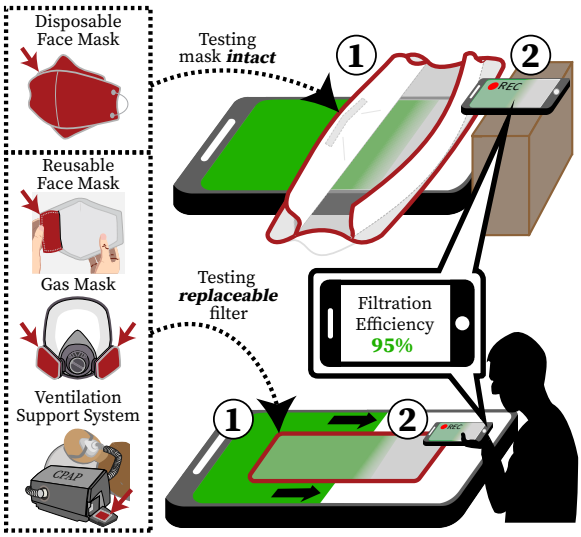

Figure 1: Figure depicts how *FilterOp* operates. The user ① places an instance to test (e.g., a disposable face mask or a replaceable filter) on a smartphone display, and ② takes a video recording (using a second smartphone) of the display projecting a colored rectangle moving from left to right. *FilterOp* utilizes the *optical* properties, namely light *absorption* and *scattering* to predict the filtration efficiency.

representation of PFEs [26, 42]. ***(3) Lack of Filter Verification Method for the Average Users:*** Furthermore, an average user lacks access to adequate tools, techniques, and knowledge to independently verify the filtration efficiency of filters. Unlike regulatory bodies or specialized laboratories that utilize expensive state-of-the-art testing machines (see § 2.2), individuals typically lack the means to perform such assessments [1, 2]. Consequently, they are left solely to rely on the information provided by mask manufacturers and packaging labels, which may not always be transparent or accurate.

To overcome these problems, we ask the following question – *can we empower an average user to test the filtration efficiency with a **practical** solution that only leverages **commodity smartphones***? To this end, we propose *FilterOp* that only utilizes a smartphone camera with another display device to estimate the filtration efficiency. The core idea of *FilterOp* is that the filter *absorbs* and *scatters* the *visible light* passing through it, and the observed intensity of these effects is correlated to the filtration efficiency (hence the name *FilterOp*, utilizing *optical* properties to test filters). The filtration efficiency and optical properties of filter materials are both driven by microfiber characteristics (i.e., *filter thickness*, *fiber volume fraction*, and *diameter*).

Figure 1 depicts an overview of how *FilterOp* operates. The user ① places an instance to test (e.g., a disposable face mask or a replaceable filter) on a smartphone display, and ② takes a video recording (using a second smartphone) of the display device depicting a pattern (e.g., a colored rectangle) moving from left to right. The smartphone camera captures the light distortion via a video recording. *FilterOp* analyzes the video to predict filtration efficiency using computer vision and machine learning techniques.

Designing *FilterOp*, however, comes with the following challenges. First, the colors perceived by the smartphone camera are subject to noise introduced by environmental factors, including variations across devices (i.e., camera and display models), lighting conditions, and screen protectors on the display. To overcome this challenge, we utilize a *reference color* – i.e., color captured from the side of the display not affected by the overlaid filter layer – as a basis for comparison with the colors distorted by the filter layer. As both the reference and captured colors are collected in the same environmental condition, the noise introduced by differences in the environment can be reduced.

Second, the input video data is subject to perturbations such as variations in the filter's fiber texture and creases on the filter surfaces. This may result in incorrectly learning the relationship between the optical properties (i.e., light absorption and scattering effects) and the filtration efficiency. We overcome this challenge by examining the *model focus* – i.e., pixels with a high weightage towards the model's decision – to estimate the quality of the data collected and accept only part of the data with higher reliability.

We implement *FilterOp* and evaluate its performance by conducting comprehensive real-world experiments under varying conditions utilizing a total of 256 instances of off-the-shelf products including different types of disposable face (respirators and surgical) masks as well as replaceable filters for reusable masks, gas masks, and ventilation support systems. We compare our results against the *ground truth* measured by a government-certified testing center that uses a state-of-the-art testing machine (costing $30K USD). Our evaluation results demonstrate that *FilterOp* yields comparable filtration efficiency estimates to that of the ground truth results, with a low mean absolute error (MAE) of 2.7%.

In summary, the contributions of this paper are:

- We propose *FilterOp*, a low-cost and pervasive solution that only requires the use of *commodity smartphones* to estimate the filtration efficiency of air filters and face masks intact. *FilterOp* works by leveraging the correlation between light absorption and scattering effects of the filter and its filtration efficiency.
- We introduce the use of reference color into the design of *FilterOp* to make the system robust against varying environmental changes and the use of model focus to improve its accuracy by selecting more reliable data for testing.
- We implement and evaluate *FilterOp* through a set of comprehensive experiments. The results demonstrate that *FilterOp* is able to provide filtration efficiency estimates that are comparable to the ground truth results provided by the state-of-the-art testing machine.

2 BACKGROUND

We first present the relevant background information of *FilterOp*. Subsequently, we present a preliminary study to demonstrate *FilterOp*'s feasibility.

Figure 2: (a) illustrates the types and the use cases of face masks. Face masks are classified into respirators, surgical masks, and reusable masks. (b) and (c) illustrate the use cases of gas masks and ventilation support systems, respectively.

2.1 Filter Types and their Use Cases

Masks and air filters are widely utilized in multiple applications, as illustrated in Figure 2.

Face Masks: *Face masks* are further classified into the following three types. *(i) Respirators* – including *N95*, *KN95*, *KF94*, and *KF80* masks [26, 27] – are disposable masks designed for strong protection against hazardous particles [30, 89]. Hence, they embed filters that have high filtration efficiencies. They are worn on a daily basis by a large population during haze seasons in many cities around the world [50, 98]. In addition, the respirators are also often worn for protection against airborne contagious viral infections as witnessed in the recent COVID-19 outbreak [16, 44]. *(ii) Surgical masks* – including *KF-AD* and *ASTM 2100* masks [26, 54, 63] – are also disposal masks designed to protect against airborne particles and droplets. They embed filters that have relatively lower filtration efficiencies. Hence, surgical masks are often used in lower-risk settings (e.g., healthcare and professional cleaning) [26, 67, 95]. *(iii) Reusable masks* are another type of face mask that enable easily removable filters to be replaced without disposing of the entire mask [5, 13, 48]. The replaceable filters can vary in the filtration efficiencies that are comparable to either the respirators or the surgical masks.

Gas Masks: Moreover, *gas masks* also utilize air filters – including *P95* filters [21, 35, 75] – providing additional protection for the face and respiratory health. Professionals working in hazardous environments such as chemical industries, firefighting, and the military often rely on gas masks [8, 34, 37, 68, 79, 81].

Ventilation Support Systems: Furthermore, filters play a crucial role in *ventilation support systems* that assist the breathing of users. For example, Continuous Positive Airway Pressure (*CPAP*) machines, often used for treating sleep apnea, include filters to provide purified air as well as to protect the machine itself [15, 58, 59]. In more severe conditions such as acute respiratory distress syndrome, where patients experience significant breathing constraints, mechanical ventilators are used. In these applications, the use of air filters is critical to prevent secondary infection and inhibit the spread of infectious pathogens around the room [6, 47, 56].

2.2 Standard Testing Method

Employing industrial laboratory testing machines for filter quality certification and regulation is the de facto standard across authorities in different countries [33, 43, 84]. Figure 3 depicts how a laboratory testing machine (i.e., Automated Filter Tester 8130A-EN [84]) operates. The machine generates and injects specific types and sizes of particles (e.g., 0.4 μm paraffin oil particles to test for KF94 masks). Then, the filtration efficiency is calculated by directly measuring the percentage of particles that penetrate the filter. However, this process contaminates the tested masks or filters, making them unusable. Although the machines yield highly accurate measurements of filtration efficiencies, high cost (e.g., approximately $30K USD) and low usability severely limit the accessibility of these machines to the general public. *FilterOp* utilizes the measurements from these machines as ground truth data (with KF94 standards) to train machine learning models. *FilterOp* could generalize to different standards given corresponding ground truth data (see § 5).

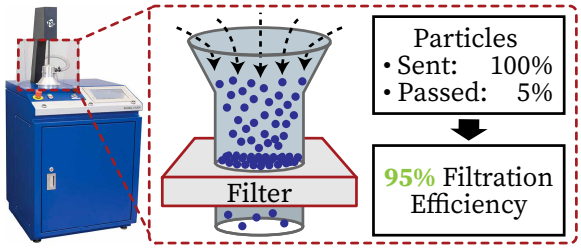

Figure 3: Figure illustrates how the state-of-the-art government-certified laboratory filter testing machine (costing over 30K USD) operates. *FilterOp* achieves comparable filtration efficiency to that of the testing machine.

2.3 Physics Model

2.3.1 Physics Model of Filtration Efficiency. When air flows through a filter, the hazardous particles come into contact with the fibers of the filter and are eventually filtered out, as depicted in Figure 4(a). The filtration efficiency of filter material is determined by the possibility of contact between particles and the fibers. Specifically, filtration efficiency (E) can be obtained from single fiber filtration efficiency (E_s), filter thickness (L), fiber volume fraction (α), and fiber diameter (d) as $E = 1 - exp(\frac{-4\alpha E_s L}{\pi d(1-\alpha)})$ [9, 10, 14, 78, 87]. This equation indicates that **thicker filters**, as well as **smaller and denser fibers**, yield **higher filtration efficiencies**.

2.3.2 Physics Model of Optical Properties. As visible light passes through the filter, the fiber *absorb* and *scatter* the light rays (see Figure 4(b)).

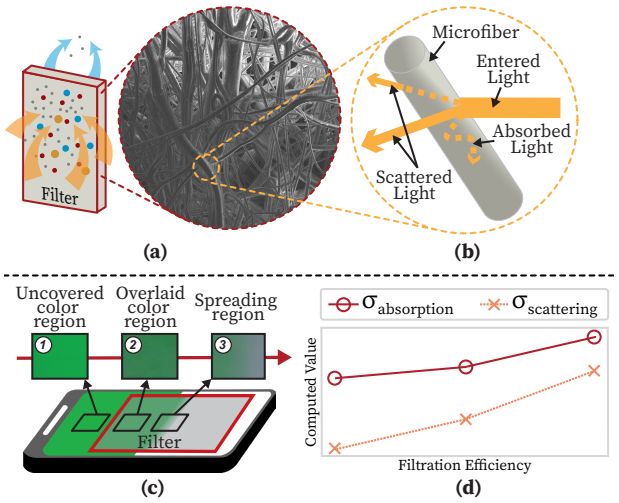

Figure 4: (a) depicts the structure of a filter densely composed of non-woven fibers. (b) depicts how a fiber *absorbs* and *scatters* light. (c) depicts the setup of the feasibility study, where the filter overlaid on a display screen attenuates and spreads the penetrated color. (d) depicts the feasibility of *FilterOp*'s core idea of utilizing light absorption and scattering effects when a filter is overlaid on a display screen. The average color difference between ① uncovered color region and ② overlaid color region ($\sigma_{absorption}$) can be attributed to light absorption. Similarly, the amount of the green color spreading towards the white color ($\sigma_{scattering}$) in ③ spreading region can be attributed to light scattering. Both values exhibit an increasing trend as the filtration efficiency of the filter increases. We advise the readers to view this figure in color.

Visible Light Absorption: Visible light absorption occurs when a light wave strikes the filter and the electrons of the material absorb the energy of the light wave and transform it into vibrational motion. The absorption causes *attenuation* of light intensity as it traverses through the fibers. The amount of attenuation increases proportionally to the **filter thickness**, **fiber volume fraction**, and **diameter** [49, 52].

Visible Light Scattering: Visible light scattering, or Mie scattering, occurs when light interacts with objects whose size is within a few orders of magnitude of the wavelength (e.g., the fiber in the filter material). This causes *spreading* of the light rays to multiple directions (forming a cone or hemisphere) [52]. As filter materials are porous, the strong contrast in refractive index between pores (i.e., air) and fibers results in strong scattering, with the light changing its direction after passing through the filter material. Hence, the amount of spreading increases as the filters become **thicker** and the fibers become **smaller** and **denser** [53].

Takeaway: We observe a correlation between the filtration efficiency and optical properties of the filter materials, with common underlying fiber characteristics (i.e., *filter thickness*, *fiber volume fraction*, and *diameter*). This is the fundamental enabler of *FilterOp*.

2.4 Feasibility Study

We conduct a preliminary experiment to test the feasibility of *FilterOp*, by checking if filters with different filtration efficiencies exhibit different optical properties (i.e., light absorption and scattering). For the preliminary experiment setup, we manually extract filters from two surgical masks with a low and medium filtration efficiency of 62.2% and 71.0%, respectively, and one KF94 mask with a high filtration efficiency of 99.9% [1]. We then place each filter on the smartphone display emitting green and white colors, overlaying the boundary between the two colors, resembling Figure 4(c). We capture the filters using a smartphone camera and examine two metrics with respect to the distortion of transmitted light: (1) the average color difference ($\sigma_{absorption}$) between ① uncovered color region and ② overlaid color region, and (2) the amount of the green color spreading towards the white color ($\sigma_{scattering}$) in ③ spreading region. For example, Figure 4(c) depicts examples of the captured regions. We compute $\sigma_{absorption}$ by finding the color distance [66] between the average colors (i.e., RGB values) of pixels in ① and ②. We then compute $\sigma_{scattering}$ using the rate of color changes per pixel as the color of each pixel in ③ changes from green to white (when viewing from left to right).

Figure 4(d) depicts computed values of $\sigma_{absorption}$ and $\sigma_{scattering}$ of filters. As the filtration efficiency increases, we observe that $\sigma_{absorption}$ increases due to the higher light absorption of the filter material. Likewise, $\sigma_{scattering}$ increases because the filters with higher filtration efficiencies tend to scatter the light more. Hence, the results align with the aforementioned physics model, verifying the feasibility of leveraging the optical properties of a filter to estimate its filtration efficiency.

3 DESIGN AND IMPLEMENTATION

We present *FilterOp*'s design and implementation details.

3.1 System Model

Goal. *FilterOp*'s *goal* is to test the filtration efficiency of filters by capturing the relevant optical properties, namely, the *light absorption and scattering effects* observed when the filter is placed between a display device and a camera.

Requirements. In designing *FilterOp*, we have the following *requirements*: (1) accurately estimate the filtration efficiency (*accuracy*); (2) minimize user involvement (*usability*); and (3) only utilize commodity devices while being robust to various environmental conditions (*deployability*).

Assumptions. We assume that *FilterOp* user owns a pair of smartphones that have a camera and a display.

3.2 System Overview

FilterOp is divided into two phases, namely *Bootstrapping* and *Verification*. *Bootstrapping Phase* occurs offline, where **government authorities or manufacturers** train the filter models from a large set of video recordings of filters with varying filtration efficiencies, along with the label, namely, the *ground truth* filtration efficiencies collected from testing machines. *FilterOp* then utilizes the trained

[1]The filtration efficiency refers to that of the entire mask.

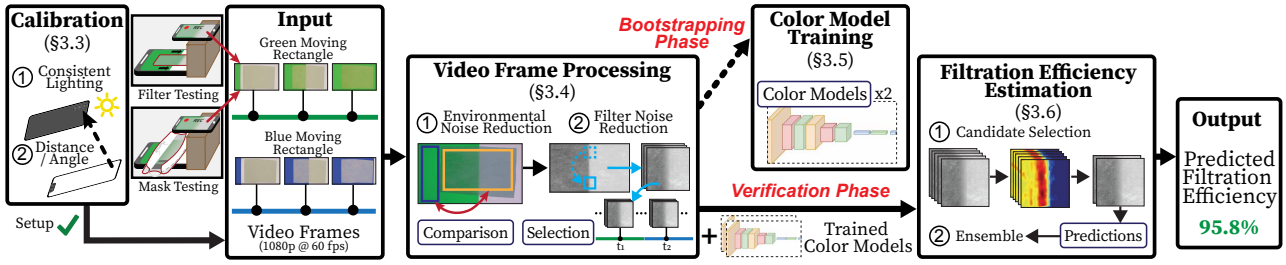

Figure 5: Figure depicts the flowchart of *FilterOp*'s design. During the *Bootstrapping Phase*, *FilterOp* trains its models to incorporate a set of video recordings of masks or air filters with their corresponding ground truth filtration efficiencies. We envision government authorities such as CDC or FDA may take part in this phase. In the *Verification Phase*, users utilize *FilterOp* on their smartphones to test their masks or replaceable filters.

model in its *Verification Phase*, occurring online as the **users** utilize the *FilterOp* app on their smartphones to test the filters.

Calibration and Input. Figure 5 illustrates an overview of *FilterOp*'s design. *FilterOp* first instructs the user, with the *Calibration* module (§ 3.3), to set up the camera and display devices within an appropriate distance and angle and checks the environment lighting condition. *FilterOp* then takes as input the video recordings (captured by a smartphone camera) of the display device with an overlaid filter. The display device projects colored rectangles (green then blue) moving from left to right, eventually filling up the entire filter and the screen. The moving rectangle allows *FilterOp* to capture the color patterns at locations along the *boundary* of the rectangle in *each frame*, and eventually examine all locations of the overlaid filter *across frames*.

Processing Pipeline. In the *Bootstrapping Phase*, *FilterOp* processes the video frames in the *Video Frame Processing* module (§ 3.4) to reduce noise from multiple sources. *FilterOp* then passes the processed frames into the *Color Model Training* module (§ 3.5), which learns how to calculate filtration efficiency based on extracted color patterns. In the *Verification Phase*, *FilterOp* processes the video frames in the *Video Frame Processing* module (§ 3.4) and then utilizes trained models to estimate the filtration efficiency in the *Filtration Efficiency Estimation* module (§ 3.6).

3.3 Calibration

As *FilterOp* utilizes captured color patterns, the colors are sensitive to camera-to-display distance, angle, and lighting conditions of the test environment. *FilterOp* requires the camera and display to be within an appropriate distance (i.e., between 10 and 15cm), angle (i.e., within five degrees), and consistent lighting conditions for optimal performance (see § 4.4.4 and § 4.4.6). We use four circles projected at the corners of the display to estimate the position of the user's smartphone camera. We then use visual cues, such as arrows and text, to guide the user to the optimal location. Subsequently, we use the smartphone's ambient light sensor to measure the intensity of the surrounding light, and the camera to detect shadows and glares on the display to alert users of inconsistent lighting. Furthermore, *FilterOp* performs this calibration process again in the *Video Frame Processing* module (§ 3.4) to ***validate every video frame***. If the condition check fails, the corresponding frame is discarded.

3.4 Video Frame Processing

FilterOp processes input video frames to capture the *absorption* and *scattering effects* of light passing through the filter. However, there are two types of noise interfering with the light signal as follows: *(1) Environmental noise:* different environmental conditions such as variations across devices (i.e., camera and display models) and screen protectors; and *(2) Filter noise:* Creases on the filter surfaces due to folding and packaging, causing air gaps between the filter and the screen. Hence, *FilterOp* reduces the resulting noise in the *Environmental Noise Reduction* (§ 3.4.1) and the *Filter Noise Reduction* (§ 3.4.2) stages. Figure 6 depicts the processing pipeline.

3.4.1 Environmental Noise Reduction. *FilterOp* aims to reduce environmental noise by utilizing the reference color – i.e., color captured from the side of the screen that is not distorted by the overlaid filter – as a basis for comparison with the captured color passing through the filter. It takes raw video frames as input and performs two processing tasks.

① Region Detection. *FilterOp* detects **in each frame** the *filter region*, R_{filter}, a bounding box of the filter overlaid on the screen. *FilterOp* also detects the *reference region*, R_{ref}, a bounding box of the screen uncovered by the filter. We observe significant differences in pixel values between R_{ref} and R_{filter}, allowing us to utilize Otsu's thresholding [64] to separate pixels in the frame into the foreground (i.e., R_{filter})/background, and contour detection algorithm [51] to eventually detect the boundary of R_{filter}. To obtain R_{ref}, we take the region to the left of the detected R_{filter}.

② Filter Region (R_{filter}) Processing. *FilterOp* processes the filter region, R_{filter}, to reduce environmental noise by comparing it with the reference region, R_{ref}. We first compute the average pixel value of R_{ref} as $Color_{ref}$ to capture the reference color and mitigate the Moiré pattern. Note that $Color_{ref}$ varies with the camera and display devices, screen protectors, and lighting conditions. We then utilize the *color distance* metric [66] which represents color differences, to compare the pixels within R_{filter} with $Color_{ref}$. For each pixel p_{ij} in R_{filter}, we compute the *color distance* which ranges from 0 to 1 (0 indicates the minimal amount of color difference and 1 indicates the maximum) to obtain a *processed filter region*, $R_{processed}$, for each frame.

3.4.2 Filter Noise Reduction. Recall that the air gaps between the filter and the screen yield additional noise. Hence, we need to only

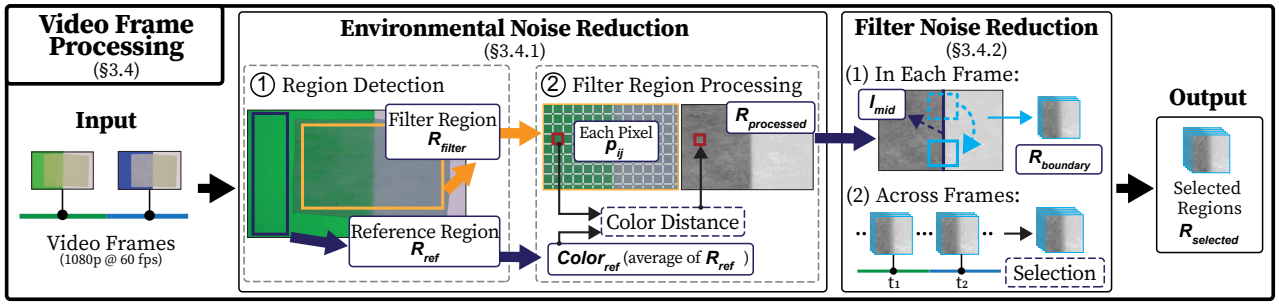

Figure 6: Figure depicts *FilterOp*'s *Video Frame Processing* module (§ 3.4), which extracts from video frames the regions capturing *light absorption* and *scattering effects*. *FilterOp* processes the regions to be robust against *environmental noise* (from variations across different camera and display devices, and screen protectors) and *filter noise* (from air gaps between the filter and the screen caused by uneven filter surfaces).

select the locations that are in close contact with the screen. We design the moving rectangles so that different frames will capture different locations over the filter, maximizing our chances of capturing the noise-free locations. Thus, we perform the following two tasks.

(1) Extracting Boundary Regions *in Each Frame.* In each frame, *FilterOp* captures *light absorption* and *scattering effects* occurring along the **boundary** of the moving color rectangle inside $R_{processed}$. We first detect the boundary of the rectangle as the **mid-line**, l_{mid}, by finding the pixels that experience the sharpest change in color. To ensure that possible regions of close contact can be found later, we utilize the sliding-window-with-overlap approach to crop out windows, $R_{boundary}$, of size 100 x 100 pixels with 50% overlap (set empirically).

(2) Selecting Regions of Close Contact *across Frames.* Across frames, $R_{boundary}$ indicates possible regions of close contact at different locations on the filter. After obtaining $R_{boundary}$ for all frames, we only select a portion of them. We observe that the amount of color difference is smaller when the filter surfaces and the screen are in closer contact. Hence, we compute the average pixel value of $R_{boundary}$ and select the lowest 50% (set empirically) as the selected regions, $R_{selected}$. *FilterOp* passes them to the *Color Model Training* module (§ 3.5) in the *Bootstrapping Phase* and the *Filtration Efficiency Estimation* module (§ 3.6) in the *Verification Phase*.

3.5 Color Model Training

FilterOp aims to (1) extract robust features on the *absorption* and *scattering effects*, and (2) learn the relationship between the extracted image features and filtration efficiency (see § 2.4) in the *Bootstrapping Phase*. It takes as input the selected regions from the *Video Frame Processing* module (§ 3.4) and outputs two machine learning models. Recall that the display pattern contains both green and blue moving rectangles. We train one model for each color. Specifically, we utilize a convolutional neural network (CNN) as the model architecture. The input image is kept small (i.e., 100 x 100 pixels), preventing the model from over-fitting the appearance and texture of the filter. To design the model architecture, there are two requirements: (1) the model should be **lightweight** and (2) the model should yield **accurate** filtration efficiency. We tune the number of convolutional layers (i.e., from two to six) to compare the output filtration efficiency in each setting. We observe that the results are comparable (i.e., the difference in the output filtration efficiency is less than 1% on average). Hence, we utilize only two convolutional layers with a 3 x 3 kernel and 16 and 32 filters, respectively, to keep the model lightweight and compact for deployment on mobile devices.

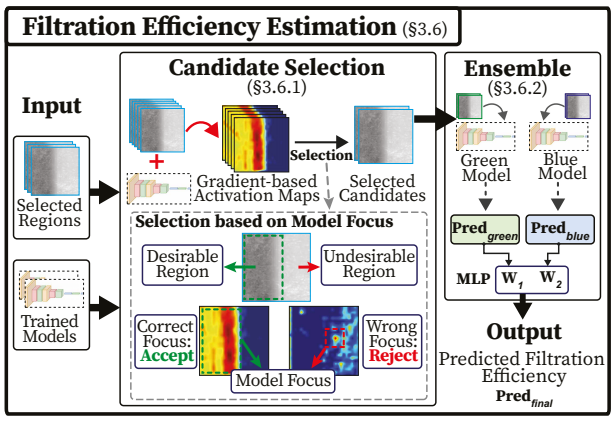

Figure 7: Figure depicts *FilterOp*'s *Filtration Efficiency Estimation* module (§ 3.6). This module examines the *model focus* – i.e., pixels with a high weightage towards the model's decision – to estimate the quality of the data collected and accept only part of the data with higher reliability.

3.6 Filtration Efficiency Estimation

FilterOp utilizes the selected regions from the *Video Frame Processing* module (§ 3.4) and trained color models from the *Color Model Training* module (§ 3.5) to estimate the filtration efficiency in the *Verification Phase*. As the selected regions from the previous stages may still contain noisy data, we identify the candidates that are likely to have less noise among the selected regions and only pass these candidates to the trained models for predictions at the *Candidate Selection* stage. Subsequently, we ensemble the predictions of

the trained color models at the *Ensemble* stage (§ 3.6.2) to obtain the final output filtration efficiency.

3.6.1 Candidate Selection. *FilterOp* identifies less noisy candidates among the *selected regions* by examining how the *trained models* assign corresponding weights to each of the pixels in the *selected regions*. We observe that the model tends to assign erroneously high weights to anomalous pixels arising from filter appearance or texture, or air gaps caused by uneven filter surfaces. To mitigate this problem, for each input image, we examine the *model focus* – i.e., pixels with a high weightage towards the model's decision – to identify candidates of less noisy regions that may yield high accuracy.

Specifically, we generate a gradient-based activation map to visualize the *model focus* for each input image. We adopt the GradCAM technique [72], often used to explain parts of the image most important to the CNNs for classification. Figure 7 depicts an example of a gradient-based activation map where the model has a correct focus. The warm colors (e.g., red and yellow) in the figure highlight the model focus. The *desirable region* is the region inside and at the boundary of the moving rectangle (see § 3.4.2). The figure also depicts an example where the model has a wrong focus outside the moving rectangle (i.e., in the *undesirable region*).

For selection, we compare the pixel values of the gradient-based activation map inside and outside the moving rectangle. We only accept an input image if the red channel of the pixels inside, which correlates to the model focus, has a higher average value than those outside.

3.6.2 Ensemble. *FilterOp* ensembles all of the intermediate predictions of the filtration efficiency to compute final *predicted filtration efficiency*. For predictions of the same color model (see § 3.5), we first compute the average prediction, i.e., $Pred_{green}$ and $Pred_{blue}$, and then combine the predictions by computing a weighted average. As different colors (e.g., green and blue) have different wavelengths, the corresponding colored light is absorbed and scattered by the filter differently. We utilize a Multi-Layer Perceptron (MLP) Regressor to learn the corresponding weights W_1 and W_2 in the weighted average, respectively. The final prediction is $Pred_{final} = W_1 Pred_{green} + W_2 Pred_{blue}$.

4 EVALUATION

This section evaluates *FilterOp* through comprehensive real-world experiments.

4.1 Experiment Setup

4.1.1 Apparatus. Figure 8 illustrates our experiment setup.

Testing Standards. Given that there are many different standards expressing filtration efficiencies (e.g., KF94 standard uses 0.4 μm paraffin oil particles, whereas ASTM 2100 standard uses 0.1 μm sodium chloride particles), we refer to all filtration efficiencies with the KF94 standard in our evaluation (unless otherwise stated). However, we note that *FilterOp* is generalizable with any other standards if trained with corresponding ground truth data (see § 5).

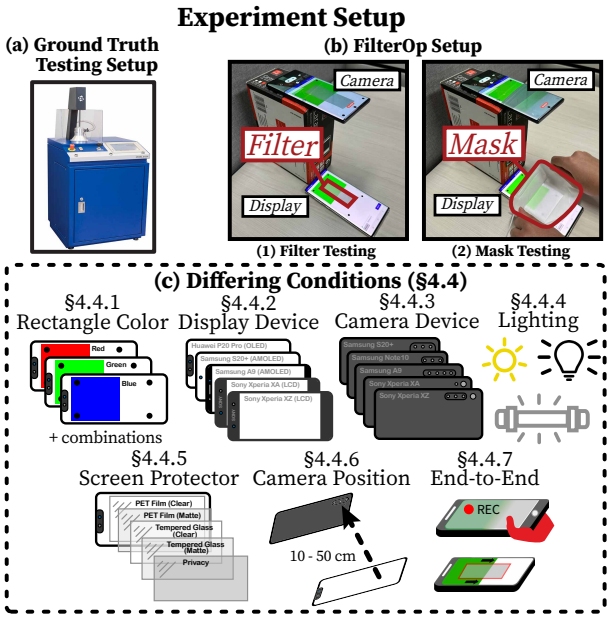

Figure 8: (a) depicts the setup (government-certified laboratory testing machine) to obtain ground truth filtration efficiency. (b) depicts *FilterOp*'s setup where we utilize two smartphones (one as a camera and the other as a display device). (c) depicts differing conditions to evaluate *FilterOp*.

***Brands* and Corresponding Advertised Standards.** We evaluate *FilterOp* with 27 different *brands* [2] including *gas masks* (P95), *respirators* (N95, KN95, KF94, and KF80), *surgical masks* (KF-AD and ASTM 2100), *reusable masks* (ASTM 2100), and *CPAP machines* (unspecified). Among the 27 *brands*, 14 advertise the P95, N95, KN95, or KF94 standards (i.e., minimum filtration efficiency of 94%) [3], four advertise the KF80 standard (i.e., minimum filtration efficiency of 80%), and seven advertise the KF-AD, ASTM 2100 or equivalent standards (i.e., minimum filtration efficiency of 70%). The remaining two *brands* have unspecified standards (i.e., minimum filtration efficiency is not guaranteed).

Ground Truth Testing. We collect the ***ground truth***, namely the filtration efficiencies measured by a government-certified testing center utilizing Automated Filter Tester 8130A-EN (costing approximately $30K USD) [84] (see Figure 8(a)). We note that the standard testing method requires testing the mask intact (i.e., all layers including *outer*, *filter*, and *inner* layers).

***Filter Testing* and *Mask Testing*.** Recall that disposable face masks (i.e., respirators and surgical masks) come equipped with an embedded filter layer (see § 2.1), while reusable masks, gas masks, and ventilation support systems utilize replaceable filters. For consistency, we evaluate *FilterOp*'s performance in two settings as illustrated in Figure 8(b):

- ***(1) Filter Testing***: *FilterOp* supports *Filter Testing*. This is to accommodate testing for the aforementioned replacement filters.

[2] We refer to *brands* as different make-and-model of masks and air filters.

[3] The N95 and KN95 masks are standardized to filter 95% of 0.3 μm particles, empirically comparable to 94% efficiency against 0.4 μm particles [46].

However, for the purpose of our evaluation, we also manually extract filter layers of disposable face masks for comprehensive evaluation (see § 4.2.2).

- ***(2) Mask Testing**: FilterOp* also supports *Mask Testing*. This is to test disposable masks ***intact*** (i.e., without extracting the filter layers).

Data Collection. We collect data over a total of 256 filter instances, namely 108 instances for *Filter Testing*, 40 instances for *Mask Testing*, and the remaining 108 instances for ground truth testing. To evaluate *FilterOp*'s overall performance, we use Samsung Galaxy Note 10 as the camera device and Huawei P20 Pro as the display device under dim room lighting. We place the filter or mask on the display device and record a video of approximately 40 seconds for each instance. We then evaluate *FilterOp* in differing conditions (see § 4.4 and Figure 8(c)). We conduct this study upon the approval of our institution's Institutional Review Board.

Training *FilterOp*. During the training of *FilterOp*'s color models (see §3.5), we utilize images extracted from the video recording of each mask and air filter (i.e., over *five thousand* images from each video recording). To prevent over-fitting on the data collected, we train the models with a small number of epochs (i.e., a maximum of *ten epochs*) and adopt the cross-validation approach to select the best model.

4.1.2 Terminology and Evaluation Metrics. We define the filtration efficiencies (FE) of filters/masks measured by the Automated Filter Tester as ***ground truth*** **(**FE_{true}**)**, and *FilterOp*'s predicted FE as ***FilterOp prediction*** **(**FE_{pred}**)**. We define *Mean Absolute Error* (*MAE*) as $\sum |(FE_{true} - FE_{pred})|/N$, where N is the number of tested instances.

4.2 Overall Performance

4.2.1 Data Preparation. To evaluate *FilterOp*'s overall performance, we test 148 filter instances across 27 *brands* (depicted in Figure 9(a)). Each *brand* has four instances. We employ the leave-one-out approach, i.e., training with 26 *brands* and testing on the remainder. We train the color models with over 130 thousand extracted images in total. Note that the test *brand* is ***unseen*** in the training.

4.2.2 Overall Results. We demonstrate *FilterOp*'s overall performance on (1) predicting the filtration efficiency of the tested filter (i.e., *Filter Testing*), (2) predicting the filtration efficiency of the mask (intact) with the filter and additional layers together (i.e., *Mask Testing*), and (3) a case study of detecting substandard masks and filters.

(1) Filter Testing. Figure 9(b) illustrates *FilterOp*'s predictions compared to the ground truth. We observe that *FilterOp* achieves accurate predictions with a low *MAE* of 2.7% across all 27 *brands*. Specifically, the *MAE* is as low as 1.8% for replacement filters, namely the ones for reusable masks, gas masks, and CPAP machines.

(2) Mask Testing. We then evaluate *FilterOp*'s performance in a practical setting for face masks intact, as wearers may not want to extract the filters, inevitably destroying the mask instance. We randomly select two representatives for N95, KN95, KF94, KF80, and surgical masks, respectively, totaling ten *brands*. For each *brand*, we then sample four instances to undergo *Mask Testing*. Figure 10 compares *FilterOp*'s predictions under *Mask Testing* with the ground truth and predictions under *Filter Testing*. We observe that *FilterOp* yields a low *MAE* of 2.5% under *Mask Testing*, which is comparable to the *MAE* of 2.8% under *Filter Testing* for the ten *brands* selected. However, we note that *FilterOp*'s predictions under *Mask Testing* are generally higher than the ground truth, leading to overestimation. We attribute this to the inevitable air gaps between multiple layers, and uneven surfaces of the inner and outer layers. The light becomes distorted after passing through the air gaps and uneven surfaces, introducing noises to *FilterOp*. Nevertheless, in spite of these distortions, *FilterOp* operates remarkably well under *Mask Testing*.

	Baseline	***FilterOp***
Accuracy (%)	84.0	**96.0**
False Positive Rate (%)	16.0	**0**
False Negative Rate (%)	**0**	4.0

Table 1: Table compares *FilterOp* against the considered baseline (i.e., advertised filtration efficiency) for detecting *substandard* masks and filters.

(3) Case Study: Detecting Substandard Masks and Filters. The ground truth testing reveals that ***four*** out of 25 *brands* depict filtration efficiencies significantly below their advertised standards (stated on their packaging). We now evaluate *FilterOp*'s performance in detecting such *substandard* masks and filters. To compare *FilterOp*'s performance, we set the *baseline* to be the advertised filtration efficiency. This resembles the real-world scenario where consumers rely on the information stated on the packaging.

We use the following metrics to evaluate the *baseline* and *FilterOp*. (1) *Accuracy* reports the percentage of *brands* correctly classified as legitimate, (2) *False Positive Rate* reports the percentage of substandard *brands* that are misclassified as legitimate, and (3) *False Negative Rate* reports the percentage of legitimate *brands* that are misclassified as substandard.

Table 1 depicts the comparison, where *FilterOp* yields an accuracy of 96.0%, with no false positive, but with a relatively small false negative rate of 4.0%. On the other hand, the baseline results yield a much lower accuracy of only 84.0% and a higher false positive rate of 16.0%. The results show that *FilterOp* correctly detects ***all*** *four substandard masks and filters* out of a total of 25 *brands* tested. In the given scenario, even a low false positive rate can prove to be catastrophic by misguiding the user to trust a *substandard* mask or filter, putting their health at high risk. False negatives, on the other hand, are not as critical since *FilterOp* underestimates the filtration efficiency, letting the user decide whether to continue using them. We note that ***FilterOp* does not tolerate false positives** in order to safeguard consumers' health. At the same time, the false negatives remain low.

In addition, *FilterOp* also correctly detects ***all*** *two substandard face masks* out of 10 *brands* tested under *Mask Testing*, as depicted in Figure 10. This highlights *FilterOp*'s practicality to detect *substandard face masks* before wearing them, safeguarding the wearer's health.

4.3 Module Evaluation

We evaluate the effectiveness of *FilterOp*'s internal modules.

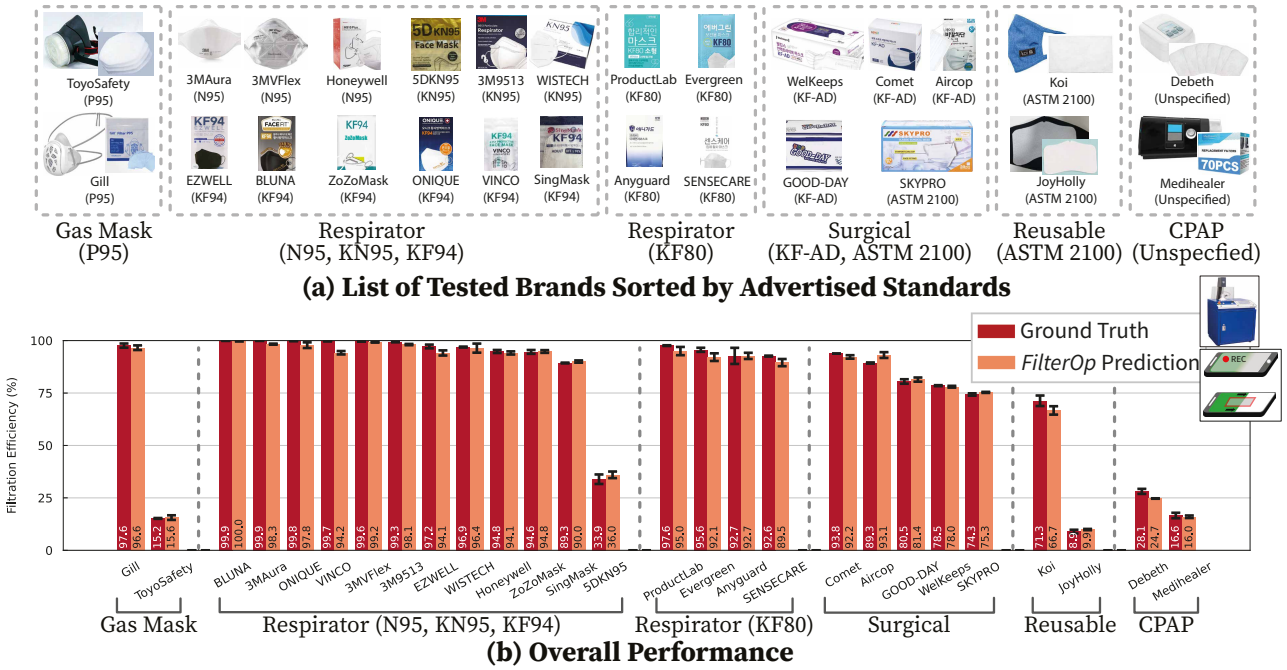

Figure 9: (a) depicts the list of 27 tested *brands* across various standards sorted by their corresponding advertised standards. (b) depicts the overall performance of *FilterOp* for *Filter Testing* compared to the ground truth.

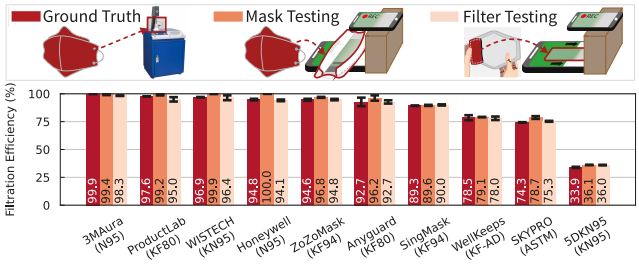

Figure 10: Figure depicts filtration efficiencies of *FilterOp* for *Mask Testing* and *Filter Testing*, also compared to the ground truth. We note that both testing methods yield comparable results.

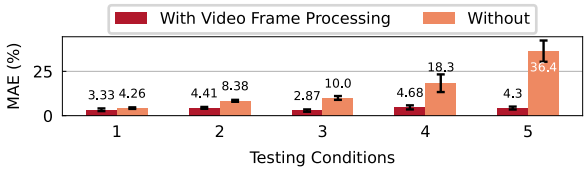

Figure 11: Figure depicts the *MAE* with/without the *Video Frame Processing* module (§ 3.4). To evaluate the effectiveness of the module, we operate *FilterOp* in different testing conditions.

4.3.1 Video Frame Processing Module. Recall that the main goal of the *Video Frame Processing* module (§ 3.4) is to enhance *FilterOp*'s robustness to testing conditions. We now compare the performance of *FilterOp* trained using video frames *with* and *without* the module, under five different testing conditions. From Figure 11, we observe that *FilterOp* trained *without* the module yields significantly large *MAE* under different conditions. We attribute such large errors to the CNN's sensitivity to significant changes in pixel values caused by variations in testing conditions, highlighting the importance of *FilterOp*'s *Video Frame Processing* module.

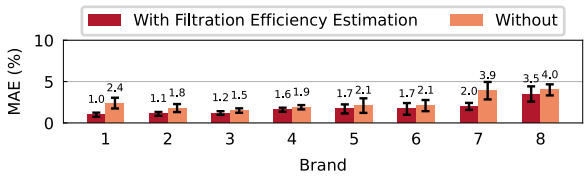

Figure 12: Figure depicts the *MAE* with/without the *Filtration Efficiency Estimation* module (§ 3.6).

4.3.2 Filtration Efficiency Estimation Module. Recall that we select candidate regions and ensemble predictions of the trained models in the *Filtration Efficiency Estimation Module* (§ 3.6). We now compare the performance of *FilterOp with* and *without* the module. Without the module, we resort to passing *all* selected regions (see § 3.4) into the trained models. We observe in Figure 12, that for all tested *brands*, the *MAE* is higher when *all* regions are used to calculate the final filtration efficiency. We attribute this to the erratic predictions when the model focuses on undesirable regions such as the texture of filter materials, highlighting the importance of *FilterOp*'s *Filtration Efficiency Estimation* module.

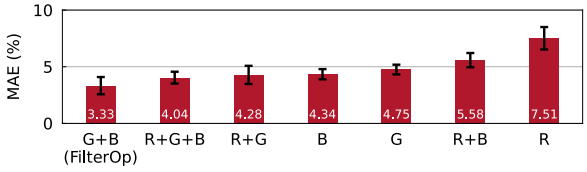

Figure 13: Figure depicts the *MAE* with varying displayed rectangle colors.

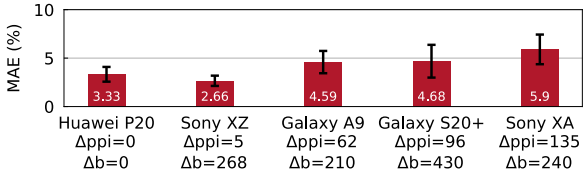

Figure 14: Figure depicts the *MAE* with varying display devices and specifications, such as pixel density (*ppi*) and brightness (*b*).

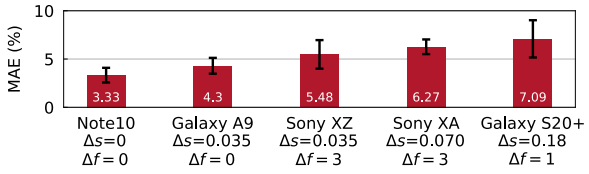

Figure 15: Figure depicts the *MAE* with varying camera devices and specifications, such as image sensor size (*s*) and focal length (*f*).

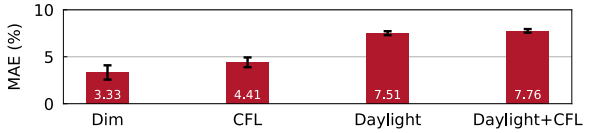

Figure 16: Figure depicts the *MAE* with varying lighting conditions.

4.4 Differing Conditions

We evaluate the robustness of *FilterOp* against different usage conditions. Specifically, we train *FilterOp* under the same conditions as § 4.2 (i.e., using Samsung Galaxy Note 10 as the camera device and Huawei P20 Pro as the display device under dim room lighting). We adopt the leave-one-brand-out approach. We then test *FilterOp* under varying experimental and environmental conditions. For all the experiments from § 4.4.1 to § 4.4.5, we sample five *brands* (selected at random). Subsequently, in § 4.4.7, we evaluate *FilterOp* with an *end-to-end* setup.

4.4.1 Varying Rectangle Colors. Recall that *FilterOp* captures moving colored rectangles projected by the display device. The displayed color affects the **wavelength** of the emitted light signal. We evaluate the effect of the displayed color on *FilterOp*'s performance. We first train and test *FilterOp* when the display device projects only one colored rectangle (i.e., red (R), green (G), or blue (B) corresponding to the colors of light-emitting diodes) and multiple colored rectangles projected one after the other (i.e., R+B, R+G, G+B, R+G+B). Figure 13 depicts the *MAE* of *FilterOp* with varying displayed colors. Using multiple colored rectangles generally yields lower *MAE*. However, involving the red color generally yields a higher *MAE*. We conjecture that the long wavelength of red light causes a high absorption rate (hence high signal-to-noise ratio) and large randomness in scattering, hindering *FilterOp*'s generalizability to unseen *brands*. Hence, we design *FilterOp* to only project green and blue rectangles, which yield the lowest error.

4.4.2 Varying Display Devices. Display devices usually vary in **screen type** (e.g., OLED, LED, LCD), **brightness**, **color range**, and **pixel density**. We evaluate the performance of *FilterOp* using different smartphones with varying display specifications. Among the specifications, pixel density is the most important factor. In Figure 14, we observe an increasing trend in *MAE* as the ***difference in screen pixel density*** (i.e., Δppi) between our training display device (i.e., Huawei P20 Pro) and other devices increases. For example, Sony Xperia XZ exhibits the lowest *MAE* because the device has a pixel density of 424ppi, similar to Huawei P20's 429ppi (i.e., $\Delta ppi = 5$). Brightness, however, does not have a significant impact on *FilterOp*'s performance. There is no observable trend in the ***difference in screen brightness*** (i.e., Δb in nits). Overall, *FilterOp* yields *MAE* below 6% for all tested devices, generalizing well to different display specifications.

4.4.3 Varying Camera Devices. Similarly, smartphone cameras also have different specifications. We evaluate *FilterOp* using different smartphones with varying **image sensor size** and **focal length**, which may impact the overall image quality like brightness and sharpness. From Figure 15, both image sensor size and focal length contribute to the increase in *MAE*, but image sensor size plays a more important role. We define Δf (mm) and Δs (inch) as the difference in focal length and image sensor size, respectively, between the training device and other devices. For example, Samsung Galaxy A9 (i.e., $\Delta f = 0$ and $\Delta s = 0.035$) has the lowest *MAE*, and Samsung Galaxy Note 10 (i.e., $\Delta f = 1$ and $\Delta s = 0.18$) has the highest *MAE* of 7.09%. Despite some variations, *FilterOp* generalizes well across different camera devices.

4.4.4 Varying Lighting Conditions. We evaluate *FilterOp*'s performance in different lighting conditions. Figure 16 depicts the *MAE* under different combinations of natural daylight and compact fluorescent lights (CFL). We observe an increasing trend in the *MAE* as the **ambient lighting** intensifies, with the highest *MAE* of 7.76% in the Daylight+CFL scenario. We attribute such performance degradation to the strong reflections off the filter, overshadowing the intended effects. To capture the intended effects with minimal noise, *FilterOp*'s *Calibration* module checks the intensity of ambient lighting conditions and instructs the user to perform testing under conditions similar to dim and CFL lighting.

4.4.5 Varying Screen Protectors. We evaluate the effects of the screen protectors on *FilterOp*'s performance. We apply a variety of protective films on the display device. These include (1) clear Polyethylene Terephthalate (PET) film, (2) PET film with a matte

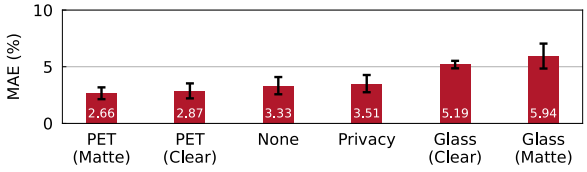

Figure 17: Figure depicts the *MAE* with varying types of screen protectors.

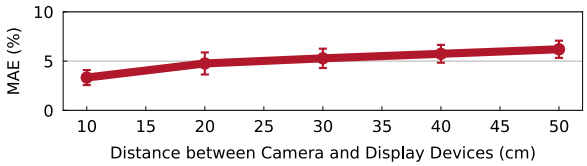

Figure 18: Figure depicts the *MAE* with varying camera-to-display distances.

Figure 19: Figure depicts the *MAE* in the practical (handheld setup) and optimal (static setup) conditions.

finish, (3) clear tempered glass, (4) matte tempered glass, and (5) privacy-preserving protectors that employ a polarized sheet to reduce viewing angle. From Figure 17, we observe that *FilterOp* has no substantial increase in *MAE* for the PET films and privacy-preserving protectors. The tempered glass protectors, however, demonstrate a slight increase in *MAE* by around 2.5%. We attribute this increase to the thicker glass protectors, which cause (unwanted) additional absorption and scattering of light.

4.4.6 Varying Camera Positions. We evaluate *FilterOp* against changing the distance and angle between the camera and the display devices. We observe in Figure 18, that *FilterOp* achieves low *MAE* within a distance of 15cm. A further increase in the distance leads to performance degradation due to a limited number of pixels captured. Furthermore, we observe that *FilterOp* yields erratic predictions if the angle is beyond five degrees. This is because the camera captures different amounts of light at different angles. *FilterOp* requires the angle to be within a tolerable range (five degrees in this case). Hence, *FilterOp*'s *Calibration* module guides the user to place the camera device to be within 10 to 15cm away from the display device and within an angle of five degrees, to achieve optimal performance.

4.4.7 End-to-End Experiment. To evaluate the practicality and usability of *FilterOp*, we invite five participants (i.e., three males and two females with ages between 20 and 30) to operate *FilterOp* by holding the camera device in a typical office lighting condition. Note that all five participants have experience using smartphones but no prior experience using *FilterOp*. We observe in Figure 19, that the performance of *FilterOp* remains comparable under both practical (i.e., Handheld+Normal Lighting) and optimal conditions (i.e., Static+Dim Lighting). *FilterOp* only has a slight performance degradation of 0.89% in *MAE*. We attribute this to the *Calibration* module (see § 3.3), which guides the user to the appropriate distance and angle and validates the testing condition in every video frame. Hence, minute hand movements and usage variations have minimal impact on performance. In addition, to evaluate the usability of the *Calibration* module, we measure the calibration time taken by each participant. We note that all participants could calibrate *FilterOp* within a minute, and the average calibration time is approximately 40 seconds.

5 DISCUSSION

We now present important discussion points of *FilterOp*.

5.1 Deployment Considerations

We discuss important considerations if *FilterOp* is to be deployed.

Further Improvement of *FilterOp*. Based on the estimated filtration efficiency of the tested mask or filter, we envision *FilterOp* to provide users with recommendations for safe applications (e.g., safe to wear for healthcare or cleaning purposes but not for protection against haze). This would significantly help users who are often confused and have no choice but to rely on the filtration efficiency labeling on the packaging, which is often inaccurate or less transparent. Furthermore, we envision a user guidance module based on augmented reality [36, 69] could be adopted to further improve the usability of *FilterOp* and remind users to keep the camera device within the appropriate range of distance and angle.

Training *FilterOp*. We implement *FilterOp* by training its model with ground truth data utilizing the KF94 standard. However, we note that *FilterOp* is generalizable to any standards as long as it is trained with the corresponding standards (such as N95 and ASTM 2100). Users of *FilterOp* are not required to perform any training and they only need to operate *FilterOp* in the *Verification Phase*. We envision that the authorities (such as CDC, FDA, and ECDC [23, 28, 29]) would have incentives to adopt and train *FilterOp*'s model in order to thwart *counterfeit* and *substandard* products. Furthermore, training data could be collected under different usage conditions to further improve the performance and robustness of *FilterOp*.

5.2 Limitations

We discuss the limitations and future works of *FilterOp*.

Requirement of Two Smartphones. As a proof-of-concept, we implement and evaluate *FilterOp* with a pair of smartphones. The core idea of *FilterOp* could be easily extended to any pair of devices with a camera and a device (e.g., a smartphone and a tablet or a laptop). Furthermore, we envision that *FilterOp* could be operated by two users (each with a smartphone), such as between family members, colleagues, and friends.

Filter Materials. As *FilterOp* leverages the optical properties of filter materials (see §2.3), the type of the material (e.g., polypropylene and cotton) may affect *FilterOp*'s performance. Hence, to achieve optimal performance, *FilterOp* needs to be trained for each type of material.

Colored Surfaces and Paintings. Colored surfaces and paintings on masks may affect *FilterOp*'s performance when testing masks intact. The users are recommended to extract the filter layers for testing and video guidance could be provided to guide users to correctly extract the filter layers.

Product Defects. *FilterOp* is not designed to detect defects in the mask and air filter products due to poor design and manufacturing errors (e.g., loose ear-loops). We envision that *FilterOp* could work in complement to existing defect detection solutions [22, 41, 90] in order to detect *substandard* products.

5.3 Extension and Impact of *FilterOp*

We discuss the extension and impact of *FilterOp*.

Other Usage Scenarios. *FilterOp* may be extended to other usage scenarios as well. For example, manufacturers do not have adequate methods of inspecting every single instance of their produced filters. This is because the state-of-the-art testing method inevitably contaminates the filters [84], rendering them useless. Hence, they rely on sampling a few sample filters in their production [65]. We envision mask and filter manufacturers incorporating an automated screen and camera in the conveyor belt of their production assembly line to deploy *FilterOp* to quickly and accurately verify every instance of their products.

Manufacturing Defects on Filters. Manufacturing defects may occur on filters due to manufacturing errors. For example, some filters may have non-homogeneous fiber density (i.e., some regions have low fiber density and some have high fiber density), thus hindering the filtration capability. To address this issue, *FilterOp* could be extended to analyze the **distribution** of the estimated filtration efficiencies of small regions (see §3.6.2) and ultimately detect such manufacturing defects on filters.

Impact of *FilterOp*. Through *FilterOp*, we hope to encourage our research community to explore how we can enable commodity mobile devices to *capture and model observable physical properties* to uncover seemingly hidden information. This way, we hope to inspire other researchers to generalize *FilterOp* to a wide range of related but novel problems including light, liquid, and material sensing.

6 RELATED WORK

We present prior work on mask testing and material sensing.

Other Mask Testing Solutions. Industrial mask testing machines provide an accurate analysis of mask quality [43, 84]. Given their high costs, researchers propose cheaper alternatives [55, 71]. However, these techniques rely on submicron particle generation and counting, requiring specialized hardware, and hence cannot be widely used by an average user. *FilterOp*, however, is a low-cost and accessible solution that only requires commodity smartphones.

Material Sensing. Researchers propose to identify different types of materials (such as solid and liquid) using radio-frequency (RF) signals to analyze the dielectric properties (e.g., permittivity) [17, 24, 38, 39, 73, 74, 85, 86, 91, 92, 96, 97]. Furthermore, other lines of work also utilize cameras, time-of-flight sensors, or light sensors to capture and analyze optical properties of materials to identify their types (such as identifying whether the material is made of plastic or wood) [12, 18, 40, 70, 82, 83, 93, 94]. However, these methods only classify the types of materials, while *FilterOp* predicts the filtration efficiencies of masks and filters by analyzing minute differences in light absorption and scattering effects.

7 CONCLUSION

We present *FilterOp*, a novel mask and filter testing system utilizing commodity smartphones to estimate filtration efficiency. *FilterOp* analyzes optical properties, namely the *absorption and scattering of the light* due to the filter materials. We evaluate *FilterOp*'s performance with real-world experiments under varying conditions utilizing 256 instances of filters. We compare *FilterOp*'s results with the state-of-the-art government-certified laboratory testing machine (costing over $30K USD) and observe that *FilterOp* provides comparable results, with a low mean absolute error of 2.7%. *FilterOp* also detects *substandard masks and filters* with an overall accuracy of 96.0%.

ACKNOWLEDGMENTS

This research was partially supported by grants from the Singapore Ministry of Education Academic Research Fund Tier 1 (R-252-000-B48-114) and the National Research Foundation of Korea (NRF) Grant funded by the Ministry of Science and ICT (RS-2023-00277848).

REFERENCES

[1] Alibaba. 2022. TSI Automated Filter Tester. https://www.alibaba.com/product-detail/TSI-Automated-Filter-Tester_1600146631207.html.

[2] Alibaba. 2022. XH XHF-112 Automatic Filter Tester of Testing Equipment. https://www.alibaba.com/product-detail/XH-XHF-112-Automatic-Filter-Tester_1600265612645.html?spm=a2700.details.0.0.19815098nvOTKL.

[3] Amazon. 2023. Hygenix 3ply Disposable Face Masks PFE 99% Filter Quality Tested by a US lab (Pack of 50 Pcs). https://www.amazon.com/Hygenix-Disposable-Filter-Tested-Nelson/dp/B089TX3BPY/ref=sr_1_10?keywords=surgical+masks&qid=1688107641&sr=8-10.

[4] Amazon. 2023. KN95 Disposable Face Mask - Miuphro Multicolor KN95 Safety Masks, 5-Ply Breathable Respirator Protection Masks for Man and Women 25 Pack. https://www.amazon.com/KN95-Face-Mask-Disposable-Efficiency%E2%89%A595/dp/B08NPSFTLR/ref=sr_1_31?crid=3V60944USOIUK&keywords=KN95&qid=1688108118&sprefix=kn%2Caps%2C569&sr=8-31.

[5] Amazon. 2023. Washable & Reusable Protective Face Masks with Filter Pocket + 30PCS Replacement Filters. https://amzn.to/44kAKZW.

[6] Arzu Ari, James B Fink, and Susan P Pilbeam. 2016. Secondhand aerosol exposure during mechanical ventilation with and without expiratory filters: An in-vitro study.

[7] Alireza Bahadori. 2015. Personnel protection and safety equipment for the oil and gas industries.

[8] William S Beckett. 2002. A New York City firefighter: overwhelmed by World Trade Center dust.

[9] Ye Bian, Shijie Wang, Li Zhang, and Chun Chen. 2020. Influence of fiber diameter, filter thickness, and packing density on PM2. 5 removal efficiency of electrospun nanofiber air filters for indoor applications. *Building and Environment* 170 (2020), 106628.

[10] BTH Borgelink, AE Carchia, JF Hernández-Sánchez, D Caputo, JGE Gardeniers, and A Susarrey-Arce. 2022. Filtering efficiency model that includes the statistical randomness of non-woven fiber layers in facemasks. *Separation and purification technology* 282 (2022), 120049.

[11] Dawn Chan. 2020. Expert says substandard masks lack proper filtration against Covid-19. https://www.nst.com.my/news/nation/2020/09/625445/expert-says-substandard-masks-lack-proper-filtration-against-covid-19

[12] Justin Chan, Ananditha Raghunath, Kelly E Michaelsen, and Shyamnath Gollakota. 2022. Testing a drop of liquid using smartphone LiDAR. *Proceedings of the ACM on Interactive, Mobile, Wearable and Ubiquitous Technologies* 6, 1 (2022), 1–27.

[13] Joanne Chen. 2022. The Best Reusable Face Masks. https://www.nytimes.com/wirecutter/reviews/best-cloth-face-masks/

[14] Longfei Chen, Shirun Ding, Zhirong Liang, Lei Zhou, Hongxing Zhang, and Cuiqi Zhang. 2017. Filtration efficiency analysis of fibrous filters: Experimental and theoretical study on the sampling of agglomerate particles emitted from a GDI engine. *Aerosol Science and Technology* 51, 9 (2017), 1082–1092.

[15] Julio A Chirinos, Indira Gurubhagavatula, Karen Teff, Daniel J Rader, Thomas A Wadden, Raymond Townsend, Gary D Foster, Greg Maislin, Hassam Saif, Preston Broderick, et al. 2014. CPAP, weight loss, or both for obstructive sleep apnea. *New England Journal of Medicine* 370, 24 (2014), 2265–2275.

[16] Roger Chou, Tracy Dana, Rebecca Jungbauer, Chandler Weeks, and Marian S McDonagh. 2020. Masks for prevention of respiratory virus infections, including SARS-CoV-2, in health care and community settings: a living rapid review. *Annals of internal medicine* 173, 7 (2020), 542–555.

[17] Ashutosh Dhekne, Mahanth Gowda, Yixuan Zhao, Haitham Hassanieh, and Romit Roy Choudhury. 2018. Liquid: A wireless liquid identifier. In *Proceedings of the 16th Annual International Conference on Mobile Systems, Applications, and Services*. Association for Computing Machinery, New York, NY, USA, 442–454.

[18] Mustafa Doga Dogan, Steven Vidal Acevedo Colon, Varnika Sinha, Kaan Akşit, and Stefanie Mueller. 2021. Sensicut: Material-aware laser cutting using speckle sensing and deep learning. In *The 34th Annual ACM Symposium on User Interface Software and Technology*. Association for Computing Machinery, New York, NY, USA, 24–38.

[19] Victoria McGrane Dugan Arnett. 2020. Masks state distributed were deficient, tests show, sparking concerns among police. https://www.bostonglobe.com/2020/04/29/nation/police-fire-departments-latest-voice-concern-with-state-provided-masks/?p1=SectionFront_Feed_ContentQuery

[20] DutchNews. 2023. Company ordered to repay state €43 million for face mask failings. https://www.dutchnews.nl/news/2023/01/company-ordered-to-repay-state-e43-million-for-face-mask-failings/

[21] Robert M Eninger, Atin Adhikari, Tiina Reponen, and Sergey A Grinshpun. 2008. Differentiating between physical and viable penetrations when challenging respirator filters with bioaerosols. *CLEAN–Soil, Air, Water* 36, 7 (2008), 615–621.

[22] Peter Evanschitzky, Nicole Auth, Tilmann Heil, Christian Felix Hermanns, and Andreas Erdmann. 2021. Mask defect detection with hybrid deep learning network. *Journal of Micro/Nanopatterning, Materials, and Metrology* 20, 4 (2021), 041205–041205.

[23] U.S. Food & Drug Administration (FDA). 2023. U.S. Food & Drug Administration (FDA). https://www.fda.gov.

[24] Chao Feng, Jie Xiong, Liqiong Chang, Ju Wang, Xiaojiang Chen, Dingyi Fang, and Zhanyong Tang. 2019. WiMi: Target Material Identification with Commodity Wi-Fi Devices. In *39th IEEE International Conference on Distributed Computing Systems, ICDCS 2019, Dallas, TX, USA, July 7-10, 2019*. IEEE, Dallas, TX, USA, 700–710. https://doi.org/10.1109/ICDCS.2019.00075

[25] Mary Ellen Flanagan, Noah Seixas, Paul Becker, Brandon Takacs, and Janice Camp. 2006. Silica exposure on construction sites: results of an exposure monitoring data compilation project. *Journal of occupational and environmental hygiene* 3, 3 (2006), 144–152.

[26] US Food and Drug Administration (FDA). 2022. N95 Respirators, Surgical Masks, Face Masks, and Barrier Face Coverings. https://www.fda.gov/medical-devices/personal-protective-equipment-infection-control/n95-respirators-surgical-masks-face-masks-and-barrier-face-coverings.

[27] Centers for Disease Control and Prevention (CDC). 2022. Types of Masks and Respirators. https://www.cdc.gov/coronavirus/2019-ncov/prevent-getting-sick/types-of-masks.html.

[28] Centers for Disease Control and Prevention (CDC). 2023. Centers for Disease Control and Prevention (CDC). https://www.cdc.gov.

[29] European Centre for Disease Prevention and Control (ECDC). 2022. Considerations for the use of face masks in the community in the context of the SARS-CoV-2 Omicron variant of concern. https://www.ecdc.europa.eu/sites/default/files/documents/Considerations-for-use-of-face-masks-in-the-community-in-the-context-of-the-SARS-CoV-2-Omicron-variant-of-concern.pdf.

[30] National Institute for Occupational Safety and Health (NIOSH). 2020. Understanding respiratory protection against SARS. https://www.cdc.gov/niosh/npptl/topics/respirators/factsheets/respsars.html.

[31] National Institute for Occupational Safety and Health (NIOSH). 2022. Counterfeit Respirators / Misrepresentation of NIOSH Approval. https://www.cdc.gov/niosh/npptl/usernotices/counterfeitResp.html.

[32] National Institute for Occupational Safety and Health (NIOSH). 2022. MNPPTL Respirator Assessments to Support the COVID-19 Response. https://www.cdc.gov/niosh/npptl/respirators/testing/NonNIOSHresults.html.

[33] Parnia Forouzandeh, Kris O'Dowd, and Suresh C Pillai. 2021. Face masks and respirators in the fight against the COVID-19 pandemic: An overview of the standards and testing methods. *Safety science* 133 (2021), 104995.

[34] Fortune Business Insights. 2023. Gas Mask Market Size, Share & Industry Analysis, By Product Type (Duct Mask, Air Purifying Respirators (APRS), Powered Air Purifying Respirators (PAPRS), Self-Contained Breathing Apparatus (SCBAS), Emergency Escape Hoods), By Application (Oil and Gas, Military, Healthcare, Mining, Fire Service, Industrial Sector, Others) and Regional Forecast, 2023-2030. https://www.fortunebusinessinsights.com/gas-mask-market-103326

[35] Priya Garg, Siyan Wang, Jessica M. Oakes, Chiara Bellini, and Michael J. Gollner. 2023. The effectiveness of filter material for respiratory protection worn by wildland firefighters. , 103811 pages. https://doi.org/10.1016/j.firesaf.2023.103811

[36] Google. 2023. Google ARCore. https://developers.google.com/ar.

[37] Susan R Grayzel. 2014. Defence Against the Indefensible: the gas mask, the State and British Culture during and after the First World War. *Twentieth Century British History* 25, 3 (2014), 418–434.

[38] Unsoo Ha, Junshan Leng, Alaa Khaddaj, and Fadel Adib. 2020. Food and Liquid Sensing in Practical Environments using RFIDs. In *17th USENIX Symposium on Networked Systems Design and Implementation, NSDI 2020, Santa Clara, CA, USA, February 25-27, 2020*, Ranjita Bhagwan and George Porter (Eds.). USENIX Association, Santa Clara, CA, USA, 1083–1100. https://www.usenix.org/conference/nsdi20/presentation/ha

[39] Unsoo Ha, Yunfei Ma, Zexuan Zhong, Tzu-Ming Hsu, and Fadel Adib. 2018. Learning food quality and safety from wireless stickers. In *Proceedings of the 17th ACM Workshop on Hot Topics in Networks*. Association for Computing Machinery, New York, NY, USA, 106–112.

[40] Chris Harrison and Scott E Hudson. 2008. Lightweight material detection for placement-aware mobile computing. In *Proceedings of the 21st annual ACM symposium on User interface software and technology*. Association for Computing Machinery, New York, NY, USA, 279–282.

[41] Jingde Huang, Zhangyu Huang, and Xin Zhan. 2023. Research on defect detection method of non-woven fabric mask based on machine vision.

[42] Chua Ming Hui, Cheng Weiren, Goh Shermin, Simin Kong, Junhua Li, Bing Lim Jason Y. C., Mao Lu Wang, Suxi Xue Kun, and Yang Le. 2020. Face Masks in the New COVID-19 Normal: Materials, Testing, and Perspectives. https://spj.science.org/doi/10.34133/2020/7286735?permanently=true#tab-citations

[43] Air Techniques International. 2022. 100X AUTOMATED FILTER TESTER. https://www.atitest.com/products/100x-automated-filter-tester/.

[44] Mariachiara Ippolito, Filippo Vitale, Giuseppe Accurso, Pasquale Iozzo, Cesare Gregoretti, Antonino Giarratano, and Andrea Cortegiani. 2020. Medical masks and Respirators for the Protection of Healthcare Workers from SARS-CoV-2 and other viruses. *Pulmonology* 26, 4 (2020), 204–212. https://doi.org/10.1016/j.pulmoe.2020.04.009

[45] Christina Jewett. 2021. Health Workers and Hospitals Grapple With Millions of Counterfeit N95 Masks. https://khn.org/news/article/health-workers-and-

hospitals-grapple-with-millions-of-counterfeit-n95-masks/
[46] Hyejung Jung, Jongbo Kim, Seungju Lee, Jinho Lee, Jooyoun Kim, Perngjy Tsai, Chungsik Yoon, et al. 2014. Comparison of filtration efficiency and pressure drop in anti-yellow sand masks, quarantine masks, medical masks, general masks, and handkerchiefs. *Aerosol Air Qual. Res* 14, 3 (2014), 991–1002.
[47] Axel Kramer, Rainer Kranabetter, Jörg Rathgeber, Klaus Züchner, Ojan Assadian, Georg Daeschlein, Nils-Olaf Hübner, Edeltrut Dietlein, Martin Exner, Matthias Gründling, et al. 2010. Infection prevention during anaesthesia ventilation by the use of breathing system filters (BSF): Joint recommendation by German Society of Hospital Hygiene (DGKH) and German Society for Anaesthesiology and Intensive Care (DGAI).
[48] Ka-Po Lee, Joanne Yip, Chi-Wai Kan, Jia-Chi Chiou, and Ka-Fu Yung. 2020. Reusable face masks as alternative for disposable medical masks: factors that affect their wear-comfort. *International Journal of Environmental Research and Public Health* 17, 18 (2020), 6623.
[49] SC Lee. 1986. Radiative transfer through a fibrous medium: allowance for fiber orientation. *Journal of Quantitative Spectroscopy and Radiative Transfer* 36, 3 (1986), 253–263.
[50] Xingzhou Li and Yan Gong. 2015. Design of polymeric nanofiber gauze mask to prevent inhaling PM2. 5 particles from haze pollution.
[51] Joseph J. Lim, C. L. Zitnick, and Piotr Dollar. 2013. Sketch Tokens: A Learned Mid-level Representation for Contour and Object Detection.
[52] Tomas Linder. 2014. *Light scattering in fiber-based materials: a foundation for characterization of structural properties*. Ph.D. Dissertation. Luleå tekniska universitet.
[53] Tomas Linder, Torbjörn Löfqvist, Erik LG Wernersson, and Per Gren. 2014. Light scattering in fibrous media with different degrees of in-plane fiber alignment. *Optics Express* 22, 14 (2014), 16829–16840.
[54] Allyson Lipp. 2003. The effectiveness of surgical face masks: what the literature shows. *Nursing Times* 99, 39 (2003), 22–24.
[55] Kenneth D Long, Elizabeth V Woodburn, Ian C Berg, Valerie Chen, and William S Scott. 2020. Measurement of filtration efficiencies of healthcare and consumer materials using modified respirator fit tester setup. *PloS one* 15, 10 (2020), e0240499.
[56] Leonardo Lorente. 2012. Respiratory filters and ventilator-associated pneumonia: composition, efficacy tests and advantages and disadvantages. , 171–177 pages.
[57] Qiming Luo, Lepeng Huang, Xuanyi Xue, Zengshun Chen, Fengbin Zhou, Lihao Wei, and Jianmin Hua. 2021. Occupational health risk assessment based on dust exposure during earthwork construction. *Journal of Building Engineering* 44 (2021), 103186.
[58] Nigel Mcardle, Graham Devereux, Hassan Heidarnejad, Heather M Engleman, Thomas W Mackay, and Neil J Douglas. 1999. Long-term use of CPAP therapy for sleep apnea/hypopnea syndrome. *American Journal of Respiratory and Critical Care Medicine* 159, 4 (1999), 1108–1114.
[59] R Doug McEvoy, Nick A Antic, Emma Heeley, Yuanming Luo, Qiong Ou, Xilong Zhang, Olga Mediano, Rui Chen, Luciano F Drager, Zhihong Liu, et al. 2016. CPAP for prevention of cardiovascular events in obstructive sleep apnea. *New England Journal of Medicine* 375, 10 (2016), 919–931.
[60] Ollie Wykeham Melissa Madison. 2020. Fake face masks fail safety standards at Queensland coal mines following coronavirus high demand. https://www.abc.net.au/news/2020-07-30/fake-face-masks-risk-coronavirus-shortages-concern-union/12506164
[61] Rahman MZ, Hoque ME, Alam MR, Rouf MA, Khan SI, Xu H, and Ramakrishna S. 2022. Face Masks to Combat Coronavirus (COVID-19)-Processing, Roles, Requirements, Efficacy, Risk and Sustainability. https://www.ncbi.nlm.nih.gov/pmc/articles/PMC9003287/
[62] Mark Naylor. 2023. Hull cleaning boss jailed for selling dodgy face masks during height of Covid-19 pandemic. https://www.hulldailymail.co.uk/news/hull-east-yorkshire-news/hull-cleaning-boss-jailed-selling-8186271
[63] Tara Oberg and Lisa M Brosseau. 2008. Surgical mask filter and fit performance. *American journal of infection control* 36, 4 (2008), 276–282.
[64] Nobuyuki Otsu. 1979. A Threshold Selection Method from Gray-Level Histograms. *IEEE Transactions on Systems, Man, and Cybernetics* 9, 1 (1979), 62–66. https://doi.org/10.1109/TSMC.1979.4310076
[65] SIRIM QAS. 2022. Face Mask Testing And Certification. https://www.sirim-qas.com.my/our-services/product-certification/face-masks-testing-and-certification/.
[66] Thiadmer Riemersma. 2019. Colour Distance Metric. https://www.compuphase.com/cmetric.htm.
[67] Cole Rosengren. 2020. Masks becoming more common for collection workers despite lack of national guidance. https://www.wastedive.com/news/masks-face-coverings-coronavirus-waste-collection-workers-osha/576737/.
[68] Occupational Safety, Health Administration, et al. 2014. General respiratory protection guidance for employers and workers.
[69] Sriram Sami, Sean Rui Xiang Tan, Bangjie Sun, and Jun Han. 2021. Lapd: Hidden spy camera detection using smartphone time-of-flight sensors. In *Proceedings of the 19th ACM Conference on Embedded Networked Sensor Systems*. Association for Computing Machinery, New York, NY, USA, 288–301.
[70] Munehiko Sato, Shigeo Yoshida, Alex Olwal, Boxin Shi, Atsushi Hiyama, Tomohiro Tanikawa, Michitaka Hirose, and Ramesh Raskar. 2015. Spectrans: Versatile material classification for interaction with textureless, specular and transparent surfaces. In *Proceedings of the 33rd Annual ACM Conference on Human Factors in Computing Systems*. Association for Computing Machinery, New York, NY, USA, 2191–2200.
[71] Katherine Schilling, Drew R Gentner, Lawrence Wilen, Antonio Medina, Colby Buehler, Luis J Perez-Lorenzo, Krystal J Godri Pollitt, Reza Bergemann, Nick Bernardo, Jordan Peccia, et al. 2021. An accessible method for screening aerosol filtration identifies poor-performing commercial masks and respirators. *Journal of exposure science & environmental epidemiology* 31, 6 (2021), 943–952.
[72] Ramprasaath R. Selvaraju, Michael Cogswell, Abhishek Das, Ramakrishna Vedantam, Devi Parikh, and Dhruv Batra. 2017. Grad-CAM: Visual Explanations From Deep Networks via Gradient-Based Localization.
[73] Hailan Shanbhag, Sohrab Madani, Akhil Isanaka, Deepak Nair, Saurabh Gupta, and Haitham Hassanieh. 2023. Contactless Material Identification with Millimeter Wave Vibrometry. In *Proceedings of the 21st Annual International Conference on Mobile Systems, Applications and Services*. Association for Computing Machinery, New York, NY, USA, 475–488.
[74] Fei Shang, Panlong Yang, Yubo Yan, and Xiang-Yang Li. 2022. LiqRay: non-invasive and fine-grained liquid recognition system. In *Proceedings of the 28th Annual International Conference on Mobile Computing And Networking*. Association for Computing Machinery, New York, NY, USA, 296–309.
[75] Amit Sharma. 2000. Penetration, pressure drop, and wickering characteristics of NIOSH certified P-100 and P95 filters under heavy DOP loading.
[76] Priyanka Sharma. 2022. Zilingo Tried To Dispatch 'Millions' Of Substandard Masks To India: Health Ministry. https://www.vccircle.com/zilingotried-to-dispatch-millions-of-substandard-masks-to-india-health-ministry
[77] Caitlyn Shelton. 2022. CDC says 60 % of KN95 masks in the US are counterfeit: How to spot fakes. https://fox17.com/news/nation-world/cdc-60-of-kn95-masks-in-the-us-are-counterfeit-how-to-spot-fakes-coronavirus-covid-covid19-omicron-variant
[78] Dahua Shou, Jintu Fan, Heng Zhang, Xiaoming Qian, and Lin Ye. 2015. Filtration efficiency of non-uniform fibrous filters. *Aerosol Science and Technology* 49, 10 (2015), 912–919.
[79] Jaclyn Skurie. 2013. How Does a Gas Mask Protect Against Chemical Warfare? https://www.nationalgeographic.com/science/article/130830-gas-masks-syria-israel-chemical-warfare.
[80] Jessica Snouwaert. 2020. China confiscated over 31 million counterfeit face masks as coronavirus fears cause supply shortage and spike in demand. https://www.businessinsider.com/coronavirus-china-confiscated-over-31-million-counterfeit-face-masks-report-2020-2
[81] David Spelce, Timothy R Rehak, Richard W Metzler, and James S Johnson. 2017. Pre-World War I firefighter respirators and the US Bureau of Mines involvement in WWI. *Journal of the International Society for Respiratory Protection* 34, 2 (2017), 128.
[82] Shuochen Su, Felix Heide, Robin Swanson, Jonathan Klein, Clara Callenberg, Matthias B. Hullin, and Wolfgang Heidrich. 2016. Material Classification Using Raw Time-of-Flight Measurements. In *2016 IEEE Conference on Computer Vision and Pattern Recognition, CVPR 2016, Las Vegas, NV, USA, June 27-30, 2016*. IEEE Computer Society, Las Vegas, NV, USA, 3503–3511. https://doi.org/10.1109/CVPR.2016.381
[83] Bangjie Sun, Sean Rui Xiang Tan, Zhiwei Ren, Mun Choon Chan, and Jun Han. 2022. Detecting counterfeit liquid food products in a sealed bottle using a smartphone camera. In *Proceedings of the 20th Annual International Conference on Mobile Systems, Applications and Services*. Association for Computing Machinery, New York, NY, USA, 42–55.
[84] TSI. 2022. Automated Filter Tester 8130A. https://tsi.com/products/filter-testers/automated-filter-tester-8130a/.
[85] Ju Wang, Jie Xiong, Xiaojiang Chen, Hongbo Jiang, Rajesh Krishna Balan, and Dingyi Fang. 2017. TagScan: Simultaneous target imaging and material identification with commodity RFID devices. In *Proceedings of the 23rd Annual International Conference on Mobile Computing and Networking*. Association for Computing Machinery, New York, NY, USA, 288–300.
[86] Ju Wang, Jie Xiong, Xiaojiang Chen, Hongbo Jiang, Rajesh Krishna Balan, and Dingyi Fang. 2019. Simultaneous material identification and target imaging with commodity RFID devices. *IEEE Transactions on Mobile Computing* 20, 2 (2019), 739–753.
[87] Q Wang, B Maze, H Vahedi Tafreshi, and B Pourdeyhimi. 2006. Approaches for predicting collection efficiency of fibrous filters. *Journal of Textile and Apparel Technology and Management* 5, 2 (2006), 1–7.
[88] Holly Williams. 2020. How shoddy masks are getting to the front lines of the coronavirus pandemic. https://www.cbsnews.com/news/coronavirus-how-shoddy-masks-are-getting-to-the-front-lines/
[89] Kerri Wizner, Andrea Steege, and Jim Boiano. 2016. Health and Safety Practices Survey of Healthcare Workers (HCW): When are HCWs using respiratory protection.
[90] Jimyeong Woo and Heoncheol Lee. 2022. Nonlinear and Dotted Defect Detection with CNN for Multi-Vision-Based Mask Inspection. *Sensors* 22, 22 (2022), 8945.

[91] Binbin Xie, Jie Xiong, Xiaojiang Chen, Eugene Chai, Liyao Li, Zhanyong Tang, and Dingyi Fang. 2019. Tagtag: material sensing with commodity RFID. In *Proceedings of the 17th Conference on Embedded Networked Sensor Systems*. Association for Computing Machinery, New York, NY, USA, 338–350.

[92] Hui-Shyong Yeo, Gergely Flamich, Patrick Schrempf, David Harris-Birtill, and Aaron Quigley. 2016. Radarcat: Radar categorization for input & interaction. In *Proceedings of the 29th Annual Symposium on User Interface Software and Technology*. Association for Computing Machinery, New York, NY, USA, 833–841.

[93] Hui-Shyong Yeo, Juyoung Lee, Andrea Bianchi, David Harris-Birtill, and Aaron Quigley. 2017. Specam: Sensing surface color and material with the front-facing camera of a mobile device. In *Proceedings of the 19th International Conference on Human-Computer Interaction with Mobile Devices and Services*. Association for Computing Machinery, New York, NY, USA, 1–9.

[94] Shichao Yue and Dina Katabi. 2019. Liquid testing with your smartphone. In *Proceedings of the 17th Annual International Conference on Mobile Systems, Applications, and Services*. Association for Computing Machinery, New York, NY, USA, 275–286.

[95] ZenBusiness. 2021. Why You Need To Wear A Face Mask While Cleaning. https://www.zenbusiness.com/blog/why-you-need-to-wear-a-face-mask-while-cleaning/.

[96] Dingtian Zhang, Jung Wook Park, Yang Zhang, Yuhui Zhao, Yiyang Wang, Yunzhi Li, Tanvi Bhagwat, Wen-Fang Chou, Xiaojia Jia, Bernard Kippelen, et al. 2020. OptoSense: Towards ubiquitous self-powered ambient light sensing surfaces. *Proceedings of the ACM on Interactive, Mobile, Wearable and Ubiquitous Technologies* 4, 3 (2020), 1–27.

[97] Diana Zhang, Jingxian Wang, Junsu Jang, Junbo Zhang, and Swarun Kumar. 2019. On the feasibility of wi-fi based material sensing. In *The 25th Annual International Conference on Mobile Computing and Networking*. Association for Computing Machinery, New York, NY, USA, 1–16.

[98] Sini Zhang, Lingling Li, Wei Gao, Yujie Wang, and Xin Yao. 2016. Interventions to reduce individual exposure of elderly individuals and children to haze: a review. *Journal of thoracic disease* 8, 1 (2016), E62.